Article:
Wang, C, Zhou, L, Zhang, X et al. (3 more authors) (2018) The Role of Solvent Composition and Polymorph Surface Chemistry in the Solution-Mediated Phase Transformation Process of Cefaclor. Industrial & Engineering Chemistry Research, 57 (49). pp. 16925-16933. ISSN 0888-5885

https://doi.org/10.1021/acs.iecr.8b04462

The Role of Solvent Composition and Polymorph Surface Chemistry in the Solution-Mediated Phase Transformation Process of Cefaclor

Chang Wang[†], *Ling Zhou*[†], *Xia Zhang*[†], *Yongfan Yang*[†], *Qiuxiang Yin*[†, ‡, *] *Kevin J. Roberts*[§, **]

†School of Chemical Engineering and Technology, State Key Laboratory of Chemical Engineering, Tianjin University. ‡ Collaborative Innovation Center of Chemical Science and Chemical Engineering (Tianjin), Tianjin 300072, People's Republic of China. § Centre for the Digital Design of Drug Products, School of Chemical and Process Engineering, University of Leeds, LS2 9JT, U.K.

*Corresponding author. Tel.: +86-22-27405754; Fax: 86-22-27314971.

**Corresponding author. Tel.: +44 (0) 113 34 32408; Fax: 32384.

E-mail addresses: qxyin@tju.edu.cn (Qiuxiang Yin); K.J.Roberts@leeds.ac.uk (Kevin J. Roberts)

ABSTRACT

The solution-mediated phase transformation process from cefaclor dihydrate to an ethanol-water solvate is analyzed by optical microscopy, powder X-ray diffraction, scanning electron microscopy and molecular modelling. The solution concentration and polymorphic composition during slurry transformation, as monitored using UV and Raman spectroscopy, respectively, reveal that the dihydrate transforms to the ethanol-water solvate at a low ethanol concentration in the mixture solvent. The transformation process is controlled by the growth of ethanol-water solvate, which nucleates on the surfaces of the dihydrate crystals. Molecular simulation confirms the critical point of transformation between the dihydrate and the ethanol-water solvate, consistent with the experimental results. The results demonstrate the importance of the solvent composition and surface chemistry of dihydrate in promoting the heterogeneous nucleation of ethanol-water solvate and provide guidance for the process control for the target form of cefaclor required.

Keywords: Solution-mediated phase transformation, cefaclor, molecular modelling, solvate, nucleation, surface chemistry

1. INTRODUCTION

Organic solvates form a part of the solid-form landscape examined when industry selects a suitable crystal form for subsequent formulation into a drug product.[1-3] Compared to un-solvated forms, solvates may exhibit a range of different physicochemical properties such as differences in shape, melting point, solubility, stability, dissolution rate, fluidity and bioavailability.[4-5] There can also be significant effects on drug efficacy when solvates undergo desolvation due to changes in the temperature and humidity of the surroundings. A number of researchers have attempted to identify and clarify their structural properties and transformation behaviors.[6-11]

An important method for studying the formation mechanism of solvates is through solution-mediated phase transformations (SMPT) as monitored by in- or ex-situ process analytical technology.[1,7] Generally, SMPT follows Ostwald's Rule [12], i.e. reflecting the fact that, metastable forms trend to transform into the stable forms with time through a process which can be summarized in three key steps: (a) dissolution of the metastable material, (b) nucleation of a more stable form, and (c) growth of the stable form.[13-16] Each of these steps can, in principle, be influenced by many factors such as temperature, solvent type, solution composition and solids loading.[1, 17-18] Commonly, it is assumed that the nucleation of the more stable form is independent of the presence of the metastable form during the SMPT process.[14-15] However, the surfaces of metastable phases have been observed to exhibit a significant effect on the nucleation of the stable phases under certain conditions.[20-21] This phenomenon was recognized in crystals of urea acid by Boistelle and Rinaudo 1981,[22] who noted that an epitaxial relationship

between the anhydrous crystals formed on the surfaces of the dihydrate crystals confirming through seeded transformation from metastable dihydrate form crystals at low supersaturations. Similarly, Davey et al.[23-24] studied 2,6-dihydroxybenzoic acid and found that the nucleation of the stable form 2 had consistently taken place on the (001) surfaces of the metastable form 1. Stoica et al.[25] observed the heterogeneous epitaxial nucleation and growth of the steroidal polymorphic compound 7αMNa, discovering that the stable form always grew on the (010) face of the metastable form at relatively low supersaturations. Maher et al.[26] speculated that the nucleation behavior of the stable form of piracetam form III was probably surface mediated when it was noticed that a smaller particle size for the metastable form II could enhanced the nucleation rate of the stable form. Du et al.[18] concluded that the nucleation of prasugrel hydrochloride form I had occurred on the surfaces of form II, confirming that the solid loading appeared to have no influence on the phase transformation rate. Ferrari and Davey[27] pointed out that the β form L-glutamic acid nucleates on the α form surfaces, noticing also that seeding of the system with α crystals could reduce of the induction time and increase the nucleation of the β form. The underlying theory related to the mechanism by which the metastable polymorph surfaces induce the nucleation of a new phase has been interpreted in a number of ways. Boistelle and Rinaudo[22] attributed nucleation on the surfaces of a metastable form to be due to an epitaxial relationship between the two phases. Davey et al.[23-24] speculated that the higher local supersaturation was present at the surface of form 1 due to the dissolution, leading in turn to an enhancement of the heterogeneous nucleation. Olmsted et al.[28] considered that nucleation and growth of a

stable phase on crystalline substrates reflected a delicate balance between chemical and epitaxial interactions. Chadwick et al.[29] demonstrated that the molecular functionality of crystalline substrates rather than epitaxial lattice matching was the primary factor in promoting the heterogeneous nucleation of acetaminophen. Hammond et al.[30] concluded that the epitaxial nucleation of the β form on the surfaces of the α form of L-glutamic acid reflected the relatively large number of inter-particle H-bonds per unit area formed between the interacting surfaces.

Although all these studies suggested that the surfaces of an existing metastable form could induce the outcome of a new stable phase, the underlying mechanism for such a surface nucleation driven processes remains quite elusive. Recently, characterization of intermolecular interactions has been used to probe its role in the nucleation and growth behavior, thermodynamic properties and polymorphic transformation of crystals in organic solvents.[31] In particular, molecular simulation can also be advantageous in terms of probing the molecular origin of polymorphic transformations research that can be difficult to carry out through experimental studies.[32] Molecular dynamics (MD) simulations can, in particular, be used to shed light on the phase transformation behavior between two solid forms as well as aiding in the characterization of the nucleation probabilities of the stable phase on the surfaces of the metastable phase at the molecular level.

This research employs and integrated approach encompassing both molecular modeling and process analysis technology to quantify the role of solvent and surface chemistry in the SMPT process. The morphology of crystals can be strongly affected

by the balance between the intrinsic (bulk) and extrinsic (surface terminated) inter-molecular interactions of the structure.[33-34] Dharmayat et al.[35] and Turner et al.[36] both found that the rate-limiting step in the transformation process between polymorphs of p-aminobenzoic acid were associated with the dissolution process of the metastable form, reflecting the differences in surface chemistry of these two forms. Hence, to control the conversion of target product, it is necessary to explore the phase transformation process, surface chemistry and its underpinning transformation mechanism for the polymorphism system.

Cefaclor (Figure 1c), a second-generation cephalosporin, has been shown to be a safe and effective oral antibacterial and anti-inflammatory drug.[37-38] The chosen solid form for this material is the dihydrate (CFDH), which exhibits a well-defined prismatic morphology but which tends to be often contaminated by the presence of an ethanol-water solvate (CFES). The latter form has a much less ideal needle-like morphology and its formation appears to be related to the washing process used for purification. This paper thus reports the study of SMPT process from CFDH to CFES using a combination of UV spectroscopy, Raman spectroscopy, scanning electron microscopy (SEM) and optical microscopy together with molecular modelling.

2. EXPERIMENTAL AND SIMULATION SECTION

2.1. Materials

Cefaclor monohydrate was provided by North China Pharmaceutical Co., Ltd. and was used without further purification. The solvent used was analytical reagent grade ethanol, which was purchased from Tianjin Kewei Chemical Co., Tianjin, China. The molar purities of solvent were higher than 99.5%. Deionized water was prepared in the laboratory prior to use.

2.2. Crystallization and Characterization of CFDH and CFES

CFDH was obtained by the recrystallization of cefaclor monohydrate from aqueous solution.[39] CFES was precipitated from aqueous solutions by anti-solvent crystallization with ethanol. The procedure for this was to weigh an excess amount of cefaclor monohydrate into 100 mL water in a 500 ml double-jacketed glass vessel. Subsequently, the slurries were heated to 313.15 K for about 1 h and then fast filtered using a 0.22 μm syringe filter. The solutions were cooled to, and maintained at, 278.15 K, and afterwards 100 ml ethanol solvent was added at a flow rate of 0.5 ml/min. The sample was then isolated by filtration, washing and drying. The washing solvent was a 1:1 mixture of ethanol-water and the drying conditions used were 40℃ for 8 h in a vacuum oven. The crystals obtained were characterized by using an optical microscope equipped with an Eclipse E2000 digital camera. Powder X-ray diffraction (PXRD) patterns of the two forms were measured using a Rigaku D/max-2500 X-ray powder diffractometer (Rigaku Co., Japan) with Cu Kα radiation (λ = 1.541845 Å). The relative concentrations of the two forms in the ethanol-water mixture during the whole phase

transformation process were monitored using Raman spectroscopy (RXN2, Kaiser Optical Systems, Inc., Ann Arbor, MI).

2.3. Determination of the phase transition kinetics

Slurry experiments were carried out to determine the mole fraction of water in ethanol-water mixed solvents associated with the transformation of CFDH to the CFES solvate. The mole fraction of ethanol (x_e) in these mixed solvents was determined as follows:

$$x_e = \frac{m_e/M_e}{m_w/M_w + m_e/M_e} \quad (1)$$

where m_w, M_w and m_e, M_e represent the mass and the molecular mass of water and ethanol, respectively. A series of binary mixed solvents of ethanol-water were prepared with compositions ranging from x_e=0.1 to 1.0 with an interval of 0.1. A certain amount of CFDH was added into 20 g mixed of ethanol-water solvents to make sure that CFDH was in excess at 298.15 K. The slurries were constantly stirred for 24 h with a magnetic stirrer to ensure that the CFDH solid had completely converted. The resultant crystals were analyzed by PXRD and optical microscopy.

Due to the low solubility of CFDH as well as the challenge associated with the detection limitations of online analysis tools, UV spectroscopy was found to be the best choice measuring the solution concentration-time profile during the SMPT process. The change of solid composition was monitored by using in-situ Raman spectroscopy. The rate-determining step was confirmed by using these online and off-line analysis tools.

All transformation experiments were carried out using a 200 ml jacketed glass crystallizer with the temperature being controlled by a thermostatic bath. A mass of 1.0g CFDH and 100 g mixed solvent (x_e=0.3) was then poured into the crystallizer with an agitation speed of 300 rpm. The transformation experiments were carried out at 298.15 K. A thermostat (type 501A, Shanghai Laboratory Instrument Works Co., Ltd., China) was utilized to control the temperature of the solution to an accuracy of ±0.05 K. The Raman probe was immersed into the solution to determine and monitor the solid phase composition as well as the transformation behavior of CFDH during the SMPT process. The suspension was periodically sampled and filtered quickly through a 0.22 μm membrane. The resulting crystals were analyzed by optical microscopy and the filtrate was analyzed using UV-3010 spectrophotometer (HITACHI, Japan with a 1 cm path length cell) to determine the solution concentration during the SMPT process.

2.4. Molecular Dynamic Simulations

The unit cell of CFDH was obtained from single crystal X-ray diffraction data (CCDC reference number 1856369) which revealed CFDH to be monoclinic with two molecules per unit cell and a space group of $P2_1$, and unit cell parameters $a = 10.590$, $b = 7.104$ and $c = 12.188$ Å. The COMPASS force field with the force field together assigned charges from the FORCITE module was selected to optimize the unit cell.[40]

2.4.1. Simulations of the Supersaturated Solution

The role of solvent and solution structure in the SMPT was examined by MD simulations using the Accelrys Materials Studio (Accelrys Software Inc., US) molecular modelling system. Supersaturated solutions of cefaclor at nine different

concentrations at 298.15 K were examined, the selected numbers of ethanol, water and solute molecules are listed in Table S1 (see the Supporting Information). Periodic simulation boxes were built and energy minimization carried out followed by a 200 ps run in NPT ensemble (NPT, constant particle number, pressure, and temperature) using Andersen method[37] for the thermostat to reach equilibrium. The last frame of the NPT simulation was then used to carry out a further calculation in NVT ensemble (NVT, constant particle number, volume, and temperature) for at least 200 ps with the time step for each simulation being 1.0 fs.

To clarify the nature of the solute and solvent inter-molecular interactions between the solute (O_s), ethanol (O_e) and water (O_w, H_w) molecules, selected atomic sites as shown in Figure 1, were selected to perform the calculation of the radial distribution functions (RDFs), *g(r)*. The RDF represents the probability density of finding a particle B in a certain system at a distance *r* that was measured from a reference particle A. This approach was mainly used to quantify the intermolecular (H-Bonding) strengths associated with solute-solute, solvent-solvent and solvent-solute interactions in a qualitative way. The final radial distribution function *g(r)* was obtained from the resultant trajectory files. To analyze the *g(r)* plots quantitatively, the coordination number was also calculated as follows:

$$N_{AB} = 4\pi \int_{r_0}^{r_1} r^2 g_{AB}(r) \rho_B \mathrm{d}r \qquad (2)$$

where ρ_B represents the number density of particle B.

2.4.2. Simulations of the Adsorption on the Crystal Surface

The dominant observed crystal habit surfaces of CFDH were cleaved, extended and rebuilt into three-dimensional periodic boxes with a size larger than 30 Å. The thickness of vacuum was set to 50 Å to eliminate the influence of additional free boundaries. One molecule was initially placed randomly in the center of the selected crystal surfaces and minimized to find a proper initial position. Then MD calculations with NVT ensemble were carried out to obtain the optimal surface binding structure of a cefaclor molecule on the surface of CFDH. Ten different initial positions for the adsorption molecule were examined to ensure that the energies calculated were at the required global minimum. All the surface systems were calculated for at least 50 ps using a time step of 1 fs to reach equilibrium followed by a further 200 ps to obtain the final simulated structure. The adsorption energies of the solute molecule in the simulation boxes were calculated as follows[14,16]:

$$E_{\text{adsorption}}=E_{\text{total}}-(E_{\text{surface}}+E_{\text{adsorbate}}) \quad (3)$$

where $E_{\text{adsorption}}$ is the adsorption energy of the molecule on the surface of CFDH, E_{total} is the total energy of the surface plus the docked molecule, E_{surface} is the energy of the pure surface without docked molecule, and $E_{\text{adsorbate}}$ is the energy of docked molecule without the bulk surface. It should be mentioned that all the adsorption energies were normalized with respect to the surface area of the simulation boxes in order to compare the relative strengths of the adsorption sites easily.

3. RESULTS AND DISCUSSION

3.1 Identification of the solvates

The PXRD patterns of CFDH and CFES, provided in Figure 2, reveal characteristic peaks at 7.276˚, 8.595˚, 9.707˚, 14.336˚ for CFDH and 7.457˚, 11.905˚ for CFES, respectively. These peaks clearly exhibit specific differences which can be used to identify the solid form easily. The optical microscopy images of both forms, given in Figure 3, reveal that CFDH has a prismatic morphology whilst CFES exhibits a needle-like morphology. Figure 4 shows the Raman spectra for the two forms which highlights the fact that the two solvated forms can be successfully distinguished. In this work, the peak at 1630 cm^{-1} was selected as the characteristic peak of CFES whilst the peak at 1645 cm^{-1} was chosen to monitor the change of CFDH.

3.2. The Phase Transformation Behavior form CFDH to CFES

The phase transformation profile of CFDH in ethanol-water mixtures at 298.15 K is plotted in Figure 5. It can be seen that the transformation between CFDH and CFES took place at a relatively low content of ethanol within the solvent mixture. Specifically, when x_e was higher than 0.08, the CFES solid was found to be the more stable form whereas CFDH was the only solid phase in the solution when x_e was lower than 0.08. Mindful that the transformation rate was much slower close to $x_e = 0.08$, the SMPT experiments were performed at the higher value of $x_e = 0.30$ in this work.

As shown in Figure 6, the solution takes a relative long period to reach the saturated state of CFDH after adding CFDH in solid form. After 60 min after addition, the characteristic peak of CFDH was found to fall whilst the characteristic peak for

CFES increased, indicating the end of the induction period and that the nucleation and growth of CFES was taking place. However, this induction time was observed to be very short, once the solution was saturated with the transformation from CFDH to CFES taking place almost instantaneously. After a period of about 100 min, the Raman peak intensities were no longer observed to change with time, indicating that the CFDH had completely transformed to CFES. These observations are consistent with the rate-determining step of SMPT for CFDH to CFES being controlled by the growth of CFES, in good agreement with previous work of O'Mahony et al.[15]

3.3 Influence of Solid Loading on the Phase Transformation Rate

Since the solid loading of CFDH might be expected to play an important role in the SMPT process, this aspect was investigated by adding 0.6, 0.8, 1.2, and 1.6 g, respectively, of CFDH into the 50 g ethanol-water mixtures (x_e=0.3) at 298.15 K. In general, the nucleation and growth rate of CFES can be considered to be constant as the supersaturation for the same conditions (solvent and temperature) were not found to change in the SMPT process.[18] Whilst, it could be speculated that the nucleation rate might depend on the solid loading, the transformation rates and induction time (see Figure 7) were not found to significantly change with any increase in solid loading. Croker et al.[20] attributed this effect to reflect that the existing phase can act as nucleation sources for the formation of stable phase, notably that this tended to take place on the surface of the metastable phase. Therefore, the transformation time should relate to the available surface per unit mass of the existing solid of CFDH.

Examination of the surface nucleation behavior of the stable form, as monitored

by using optical microscopy, revealed (Figure 8) that the CFES (with a needle-like morphology) clearly nucleated on the surfaces of the CFDH single crystals, with its nucleation propensity following with the order of {011} > {001} > {10-1}. The nucleation surfaces of the CFDH crystals were observed to change from being optically transparent to being more opaque as the transformation process to CFES continues, as would be consistent with the dehydration occurs on these surfaces. Confirmation that the needle-like form nucleated directly on the surfaces of the block-like morphology of CFDH rather than by aggregation with other CFES crystal was provided through the SEM analysis, see Figure 9 which strongly supports the fact that CFES nucleates and subsequently grows on the surfaces of the CFDH crystals.

3.4. Formation of CFES Molecules Cluster in Supersaturated Solution

Figure 10 shows the *g(r)* calculated from the MD simulation highlighting the dominant intermolecular interactions between selected atoms within the molecules present in the different ethanol-water mixtures.

Figure 10(a) provides the $g_{Ow\text{-}Ow}(r)$ data which reveals there are two distinct peaks at around 2.7 Å and 4.5 Å, respectively, which are consistent with the work of Dixit et al.[41] The amplitude of the first peak is related to water-water interactions and these increase with increasing ethanol concentration with a higher intensity than that for the corresponding peak for pure water which has a similar shape and position. This increased intensity of the first peak clearly suggests that a local water structure or cluster exists within the ethanol-water mixtures.[1,41] The second peak is consistent with the existence of a hydrogen-bonded network which is exists in pure water, and has been

mainly preserved in both position and intensity for the different ethanol concentrations.

Figure 10(b) also illustrates the interaction between water and ethanol molecules by plotting the $g_{Oe\text{-}Ow}(r)$. From this it was found that the shape of the second peak close to 4.5 Å was much sharper than that in the corresponding $g_{Ow\text{-}Ow}(r)$ profile observed for pure water, indicating that the hydroxyl group of ethanol strengthens the tetrahedral structure in the water surrounding it.[42] As shown in the SEM image given in Figure 11, the hollow structure of CEFS supports such a water cluster model and that it participated in the formation of the crystal structure.

In Figure 10(c) and 10(d), the $g(r)$ plots of O_s-H_w and O_s-H_e are represented above of the intermolecular interactions between solute and solvents, respectively. The first large peak at about 1.5 Å indicates the strongest interaction in the ethanol-water mixtures which play a primary role in determining the CFDH and CFES crystal structures. The calculated coordination numbers based on the first peak are presented in Table 1. It shows that the number of water molecules surrounding the reference solute molecule decreases abruptly between $x_e = 0.1$ and $x_e = 0.3$ while a dramatic increase occurs on that of ethanol molecules. This result supports the hypothesis that CFDH is the stable form when the mole fraction of ethanol is less than 0.1 with CFES becoming the dominate form when x_e is greater than 0.3. These MD modelling data are also clearly consistent with the experimental slurry results (given in section 3.2), reinforcing the determination of the transformation point associated with the formation of the DFES ethanol-water solvate to be about $x_e = 0.08$.

3.5. Mechanism of Epitaxial Nucleation and Transformation on the Surfaces of

CFDH

The adsorption energy of a single CFES molecule on the surface of the crystal habit plane substrate of CFDH can provide an effective approach for the identification of likely sites for surface nucleation. The epitaxial ordering or adsorption ability of solute molecule to the surfaces of CFDH can be expected to be mostly determined by the surface topography and the nature of the molecular chemistry functional groups exposed at the surfaces. Examination of the surface chemistry for the dominant habit faces of CFDH, shown in Figure 12, reveals the nature of the different functional groups and their orientation as exposed on the surface. In this, chlorine atoms were found to be exposed on the surfaces of {001} whilst on the {10-1} and {011} crystal surfaces the amino and phenyl groups were exposed. Therefore, the optimum adsorption structures for the docked molecules can be expected to have different intermolecular interaction patterns for such different surfaces. As shown in Figure 13, the MD studies reveal that H-bonds are formed in each surface with adsorbed molecule, but with significant differences. When adsorbed on the {011} and {10-1} surfaces, the docked molecule can interaction with the surface through H-bonding between COO^- and NH_3^+ with two sites on {011} whilst only one on {10-1} face. In contrast, the formation of halogen bonds on the {001} face between Cl^- and NH_3^+ was predicted. The strength of such intermolecular interactions, as assessed through their corresponding adsorption energies for the three habit plane surfaces, are given in Table 2. The data show that the adsorption energies follow the sequence of {011} > {001} > {10-1}, which is consistent with the observed epitaxial order.

3.6 Summary Discussion

Drawing together experimental and simulation data, the transformation mechanism for SMPT from CFDH to CFES during processing has become increasingly clear. When the concentration of ethanol increases, water clusters tend to be formed and these become enhanced with increasing concentration in the mixtures. The increased ethanol and decreased water surrounding the solute molecules lead to the formation of the key structural synthons of the CFES ethanol-water solvate. As the solubility of CFES is less than that of CFDH, the nucleation and subsequent growth would be expected to occur on the surfaces of CFDH due to the strong adsorption ability of {011}, {001} and {10-1} faces. Such a transformation process would thus be expected to continue by consuming the CFDH solid phase constantly.

4. CONCLUSIONS

The SMPT process from CFDH to CFES as investigated by using in-situ Raman spectroscopy and UV spectroscopy reveal the induction time for CFES nucleation to be relatively short with the rate-limiting process for the transformation found to be associated with the growth of the stable CFES form. Variation of the solid loadings within the slurries were found to have little effect on the transformation time consistent with the nucleation of CFES being controlled by nucleation on the surfaces of the CFDH crystals. The propensity for nucleation and growth of CFES on the surface of CFDH was found to follow the order of {011} > {001} > {10-1}. Complementary MD simulations revealed the formation of water clusters with the increasing mole fraction of ethanol reflecting the strong intermolecular interactions between water molecules. The coordination number of water molecules around the solute molecule was found to rapidly decrease, whilst the number of ethanol molecules abruptly increased for ethanol content in the range $x_e = 0.1$ and $x_e = 0.3$, consistent with the results of slurry transformation experiments. The adsorption energies of single molecule docked on the dominate CFDH crystal habit surfaces were consistent with the epitaxial order revealed experimentally. These findings provide a profound understanding about the role of solvent composition as well as highlighting the importance of the crystal surface nucleation on an existing phase during the SMPT process. Overall, this work can be regarded as providing essential guidance for the preparation of crystalline products in their desired solid form.

ASSOCIATED CONTENT

Supporting Information

Detailed numbers of ethanol, water and solute molecules for the molecular dynamic calculations (Table S1). This material is available free of charge via the Internet at http://pubs.acs.org.

ACKNOWLEDGEMENTS

This research is financially supported by the Major National Scientific Instrument Development Project of China (No.21527812) and the Tianjin Municipal Natural Science Foundation (No. 16JCZDJC32700). One of us (KJR) gratefully acknowledges the UK's Engineering and Physical Science Research Council for the support of crystallization research at the University of Leeds through the award of a Critical Mass grant (EP/IO14446/1 and EP/IO13563/1).

AUTHOR CONTRIBUTIONS

The manuscript was written with contributions from all authors. All authors have given their approval to the final version of this manuscript.

CONFLICT OF INTEREST STATEMENT

The authors declare no conflicts of interest.

NOMENCLATURE

SMPT	Solution-Mediated Phase Transformation

MD	Molecular Dynamics
CFDH	Cefaclor Dihydrate
CFES	Cefaclor Ethanol-Water Solvate
NPT	Constant Particle Number, Pressure, and Temperature
NVT	Constant Particle Number, Volume, and Temperature
RDFs	Radial Distribution Functions
H-bonding	Hydrogen Bonding

LIST OF SYMBOLS

x_e	Mole Fraction of Ethanol
m_w	Mass of Water
M_w	Molecular Mass of water
m_e	Mass of Ethanol
M_e	Molecular Mass of Ethanol
g(r)	Radial Distribution Function
N_{AB}	Coordination Number
ρ_B	Number Density
r_1	The Final Distance
r_0	The Initial Distance
$E_{\text{adsorption}}$	Adsorption Energy
E_{total}	Total Energy
E_{surface}	Pure Surface Energy
$E_{\text{adsorbate}}$	Energy of Docked Molecule

REFERENCES

(1). Wang, G., Ma, Y., Wang, Y., Hao, H., Jiang, Y. (2015). Investigation of solution-mediated phase transformation of cefuroxime acid to its acetonitrile solvate. *Org*

Process Res. Dev. *19* (12), 1820-1825.

(2). Zhang, X., Yin, Q., Du, W., Gong, J., Bao, Y., Zhang, M., Hou, B., Hao, H. (2015). Phase transformation between anhydrate and monohydrate of sodium dehydroacetate. *Ind. Eng. Chem. Res*. *54* (13), 3438-3444.

(3). Renou, L., Coste, S., Cartigny, Y., Petit, M. N., Vincent, C., Schneider, J. M., (2009). Coquerel, G. Mechanism of hydration and dehydration of ciclopirox ethanolamine (1:1). *Cryst Growth Des*. *9* (9), 3918-3927.

(4). Cui, P., Yin, Q., Guo, Y., Gong, J. (2012). Polymorphic crystallization and transformation of candesartan cilexetil. *Ind. Eng. Chem. Res*, *51* (39), 12910-12916.

(5). Kim, Y. S., Rousseau, R. W. (2004). Characterization and solid-state transformations of the pseudopolymorphic forms of sodium naproxen. *Cryst Growth Des*, *4* (6), 1211-1216.

(6). Aitipamula, S., Chow, P. S., Tan, R. B. (2012). The solvates of sulfamerazine: structural, thermochemical, and desolvation studies. *CrystEngComm*, *14* (2), 691-699.

(7). Wang, Z., Wang, J., Dang, L. (2006). Nucleation, growth, and solvated behavior of erythromycin as monitored in situ by using FBRM and PVM. *Org Process Res. Dev*., *10* (3), 450-456.

(8). Jia, L., Zhang, Q., Wang, J. R., Mei, X. (2015). Versatile solid modifications of icariin: structure, properties and form transformation. *CrystEngComm*, *17* (39), 7500-7509.

(9). Nangia A, Desiraju G R. (1999) Pseudopolymorphism: occurrences of hydrogen bonding organic solvents in molecular crystals. *Chemical Communications*, (7): 605-606.

(10). Zhu, B., Zhang, Q., Ren, G., Mei, X. (2017). Solid-State Characterization and Insight into Transformations and Stability of Apatinib Mesylate Solvates[J]. *Cryst Growth Des*, 17(11): 5994-6005.

(11). Bērziņš, A., Trimdale, A., Kons, A., Zvaniņa, D. (2017). On the formation and desolvation mechanism of organic molecule solvates: a structural study of methyl cholate solvates. *Cryst Growth De*, 17(11), 5712-5724.

(12). Ostwald, W. (1897). Studies on the formation and transformation of solid compounds: Report I. Supersaturation and practicing cooling. *Phys. Chem*. *22*, 289– 330.

(13). Gu, C. H., Young, V., Grant, D. J. (2001). Polymorph screening: Influence of solvents on the rate of solvent‐mediated polymorphic transformation. *J. pharm Sci*. *90* (11), 1878-1890.

(14). Liang, S. S.; Duan, X. Z.; Zhang, X. Y.; Qian, G.; Zhou, X. G. (2015). Insights into Polymorphic Transformation of l-Glutamic Acid: A Combined Experimental and Simulation Study. *Cryst Growth Des*, *15* (8), 3602-3608.

(15). O'Mahony, M. A.; Maher, A.; Croker, D. M.; Rasmuson, Å. C.; Hodnett, B. K. (2012). Examining solution and solid state composition for the solution-mediated polymorphic transformation of carbamazepine and piracetam. *Cryst Growth Des*, *12* (4), 1925-1932.

(16). Tong, Y., Wang, Z., Yang, E., Pan, B., Dang, L., Wei, H. (2016). Insights into cocrystal polymorphic transformation mechanism of ethenzamide–saccharin: a combined experimental and simulative study. *Cryst Growth Des*, *16* (9), 5118-5126.

(17). Su, W. Y.; Hao, H. X.; Barrett, M.; Glennon, B. (2010). The impact of operating parameters on the polymorphic transformation of D-mannitol characterized in situ with Raman spectroscopy, FBRM, and PVM. *Org Process Res. Dev*., *14* (6), 1432-1437.

(18). Du, W.; Yin, Q. X.; Hao, H. X.; Bao, Y.; Zhang, X.; Huang, J. T.; Li, X. (2014). Solution-mediated polymorphic transformation of prasugrel hydrochloride from form II to form I. *Ind. Eng. Chem. Res. 53* (14), 5652-5659.

(19). O'Mahony, M. A., Seaton, C. C., Croker, D. M., Veesler, S., Rasmuson, Å. C., Hodnett, B. K. (2013). Investigation into the mechanism of solution-mediated transformation from FI to FIII carbamazepine: the role of dissolution and the interaction between polymorph surfaces. *Cryst Growth Des*, *13* (5), 1861-1871.

(20). Croker, D., Hodnett, B. K. (2010). Mechanistic features of polymorphic transformations: the role of surfaces.*Cryst Growth Des*, *10* (6), 2806-2816.

(21). Artusio F, Pisano R. (2018). Surface-induced crystallization of pharmaceuticals

and biopharmaceuticals: a review. *Int. J. Pharm*., 547 190–208.

(22). Boistelle R.; Rinaudo C. (1981). Phase transition and epitaxies between hydrated orthorhombic and anhydrous monoclinic uric acid crystals. *J. Cryst. Growth*, *53* (1), 1-9.

(23). Davey, R. J.; Blagden, N.; Righini, S.; Alison, H.; Ferrari, E. S. (2002). Nucleation control in solution mediated polymorphic phase transformations: The case of 2, 6-dihydroxybenzoic acid. *J. Phys. Chem. B 106* (8), 1954-1959.

(24). Davey, R. J.; Blagden, N.; Righini, S.; Alison, H.; Quayle, M. J.; Fuller, S. (2001). Crystal polymorphism as a probe for molecular self-assembly during nucleation from solutions: the case of 2, 6-dihydroxybenzoic acid. *Cryst Growth Des*, *1* (1), 59-65.

(25). Stoica, C.; Verwer, P.; Meekes, H.; Vlieg, E.; van Hoof, P. J. C. M.; Kaspersen, F. M. (2006). Epitaxial 2D nucleation of the stable polymorphic form of the steroid 7αMNa on the metastable form: Implications for Ostwald's rule of stages. *Int. J. Pharm. 309* (1), 16-24.

(26). Maher, A., Croker, D. M., Rasmuson, Å. C., Hodnett, B. K. (2012). Solution mediated polymorphic transformation: form II to form III piracetam in ethanol. *Cryst Growth Des*, *12* (12), 6151-6157.

(27). Ferrari E S, Davey R J. (2004). Solution-mediated transformation of α to β L-glutamic acid: Rate enhancement due to secondary nucleation. *Cryst Growth Des*, 4(5): 1061-1068.

(28). Olmsted, B. K., Ward, M. D. (2011). The role of chemical interactions and epitaxy during nucleation of organic crystals on crystalline substrates. *CrystEngComm*, *13* (4), 1070-1073.

(29). Chadwick, K., Chen, J., Myerson, A. S., Trout, B. L. (2012). Toward the rational design of crystalline surfaces for heteroepitaxy: role of molecular functionality. *Cryst Growth Des*, *12* (3), 1159-1166.

(30). Hammond R B, Pencheva K, Roberts K J. (2007). Molecular Modeling of Crystal− Crystal Interactions between the α-and β-Polymorphic Forms of l-Glutamic Acid Using Grid-Based Methods. *Cryst Growth Des*, 7(5): 875-884.

(31). Beckham, G. T., Peters, B., Starbuck, C., Variankaval, N., Trout, B. L. (2007). Surface-mediated nucleation in the solid-state polymorph transformation of terephthalic acid. *J. Am. Chem. Soc*. *129* (15), 4714-4723.

(32). Santiso, E. E., Trout, B. L. (2011). A general set of order parameters for molecular crystals. *J. Chem. Phys. 134* (6), 064109.

(33). Kim, J. W., Park, D. B., Shim, H. M., Kim, H. S., Koo, K. K. (2012). Crystallization of RDX by drowning-out combined with fines dissolution and cooling process. *Ind. Eng. Chem. Res.* 51(9), 3758–3765.

(34). Han, G., Poornachary, S. K., Chow, P. S., Tan, R. B. (2010). Understanding growth morphology changes of γ-glycine and dl-alanine polar crystals in pure aqueous solutions. *Cryst. Growth Des.* 10(11), 4883–4889.

(35). Dharmayat S, Hammond, R. B., Lai X, Ma C, Purba E, Roberts K. J., Chen P., Martin E., Morris J., Bytheway R. (2008). An examination of the kinetics of the solution-mediated polymorphic phase transformation between α-and β-forms of l-glutamic acid as determined using online powder X-ray diffraction. *Cryst Growth Des*, 8(7): 2205-2216.

(36). Turner, T. D., Caddick, S., Hammond, R. B., Roberts, K. J., Lai, X. (2018). Kinetics of the Aqueous-Ethanol Solution Mediated Transformation between the Beta and Alpha Polymorphs of p-Aminobenzoic Acid. *Cryst Growth Des*, 18(2): 1117-1125.

(37). Tomas, A., Horvat, O., Kusturica, M. P., Pavlović, N., Milijašević, B., Tomić, Z., Sabo, A. (2015). Pharmacokinetics and Pharmacodynamic dosage adaptation of cefaclor in systemic infections. *Clin. Ther. 37* (8), e81.

(38). Medenecka, B., Jelińska, A., Zajac, M., Bałdyka, M., Juszkiewicz, K., Oszczapowicz, I. (2009). Stability of the crystalline form of cefaclor monohydrate and its pharmaceutical preparations. *Acta Pol. Pharm*. *66* (5), 563–569.

(39). Wang, C., Zhang, X., Du, W., Huang, Y. H., Guo, M. X., Li, Y., Zhang, Z. X, Hou, B. H.; Yin, Q. X. (2016). Effects of solvent and supersaturation on crystal morphology of cefaclor dihydrate: a combined experimental and computer simulation study. *CrystEngComm*, *18* (47), 9085-9094.

(40). H. Sun, P. Ren and J. R. Fried. (1998). The COMPASS force field: parameterization

and validation for phosphazenes. *Comput. heor. Polym. Sci.*, 8(1), 229–246.

(41). Dixit, S., Crain, J., Poon, W. C. K., Finney, J. L., Soper, A. K. (2002). Molecular segregation observed in a concentrated alcohol–water solution. *Nature*, *416* (6883), 829-832.

(42). Zhang, C., Yang, X. (2005). Molecular dynamics simulation of ethanol/water mixtures for structure and diffusion properties. *Fluid Phase Equilibria*, *231* (1), 1-10.

Figure Captions:

Figure 1. Schematic representation of 3D molecular structures of water (a), ethanol (b), cefaclor (c) highlighting the identification of central atoms used in the radial distribution functions derived from the MD simulation.

Figure 2. Powder X-ray diffraction patterns of CFDH and CFES.

Figure 3. Optical micrographs of (a) CFDH; (b) CFES highlighting their distinctive crystal morphologies.

Figure 4. Raman spectra of CFDH and CFES in ethanol-water mixed mixtures showing "finger printing" region (see inset) at 1630 cm-1 and 1645 cm-1 for CFES and CFDH, respectively.

Figure 5. The phase transformation profile identified by PXRD after 24 h for CFDH and CFES in ethanol-water mixtures at 298.15 K.

Figure 6. Relative intensities of Raman peaks at 1630 cm^{-1} for CFES (gray line) and Raman peak at 1645 cm^{-1} for CFDH (black line) and the solution concentration (red line) measured by UV spectroscopy.

Figure 7. Time-dependent Raman intensity data showing the influence of solid loading on transformation time from CFDH to CFES in ethanol-water mixed at 298.15 K.

Figure 8. Time-dependent epitaxial nucleation and growth of CFES on the surfaces of a single crystal of CFDH optical micrographs: (a) 0.5 min; (b) 1.0 min; (c) 2 min; (d) schematic showing the crystal morphology of CFDH.

Figure 9. SEM micrographs of (a) CFES epitaxial growth on the surface of CFDH, (b) CFDH epitaxial on the surface of CFES, (c) CFDH and (d) CFES.

Figure 10. The *g(r)* radial distribution function plots for MD simulations highlighting intermolecular interactions: (a) O_w-O_w; (b) O_e-O_w; (c) O_s-H_w; (d) O_s-H_e where O is for oxygen and the sub-script refer to water (w), ethanol (e) and the solute molecule (s). The mole fraction of ethanol is from 0 to 0.7 in ethanol-water mixtures.

Figure 11. SEM micrograph of the crystal of CFES showing a hollow channel existed in the structure consistent with the MD simulation results that a water cluster formed in ethanol-water mixture.

Figure 12. Intermolecular packing diagrams showing the surface termination chemistry of the {10-1}, {001} and {011} planes.

Figure 13. Surface chemistry for the dominant crystal habit planes for CFDH showing the optimal adsorption binding site for single molecules of cefaclor: (a) face {001}, (b) face {10-1}, and face {011}.

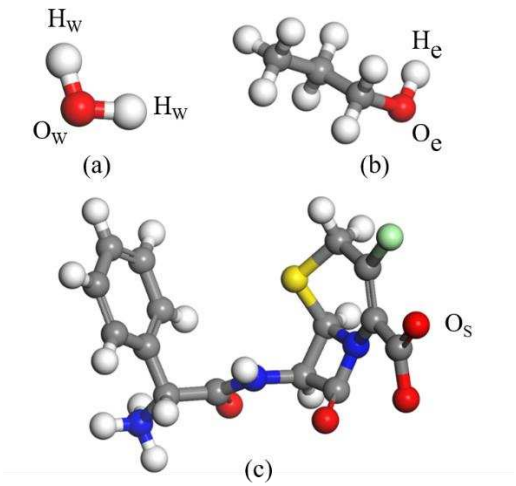

Figure 1. Schematic representation of 3D molecular structures of water (a), ethanol (b), cefaclor (c) highlighting the identification of central atoms used in the radial distribution functions derived from the MD simulation.

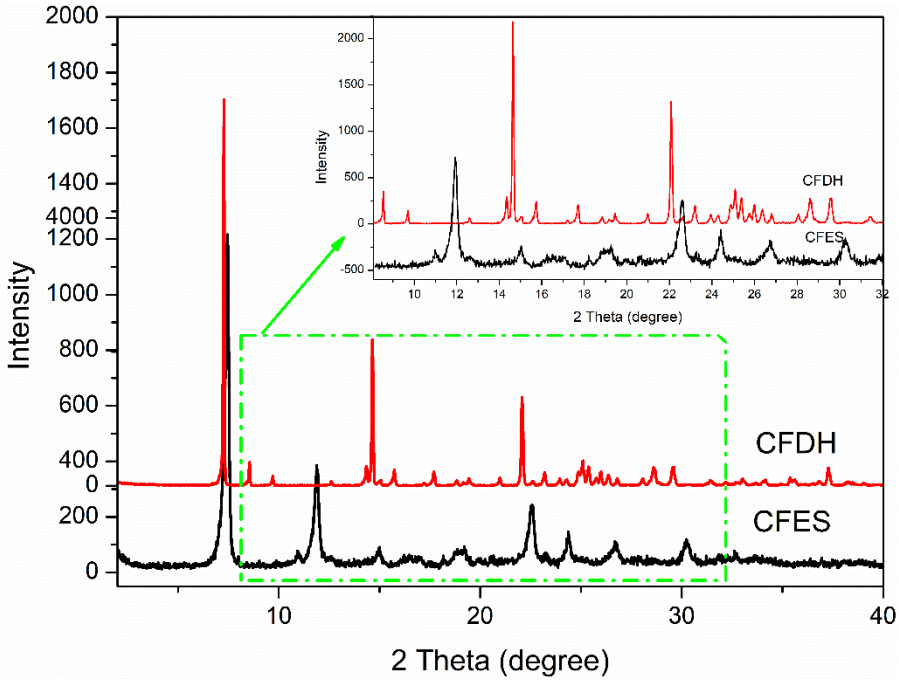

Figure 2. Powder X-ray diffraction patterns of CFDH and CFES.

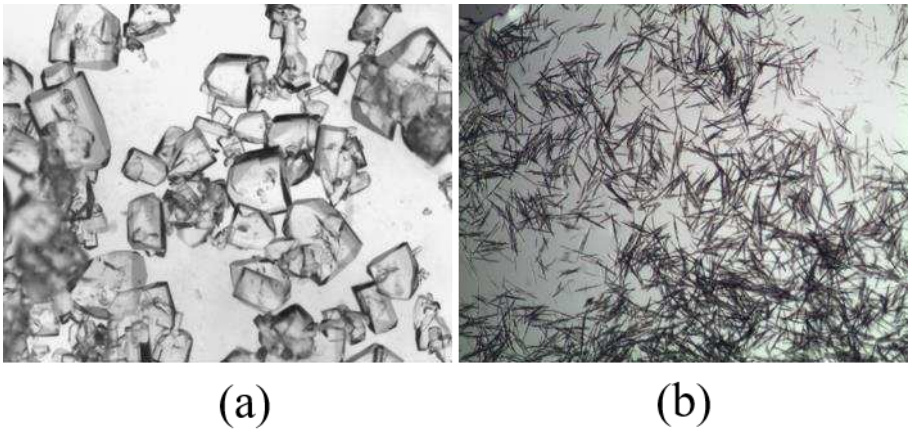

Figure 3. Optical micrographs of (a) CFDH; (b) CFES highlighting their distinctive crystal morphologies.

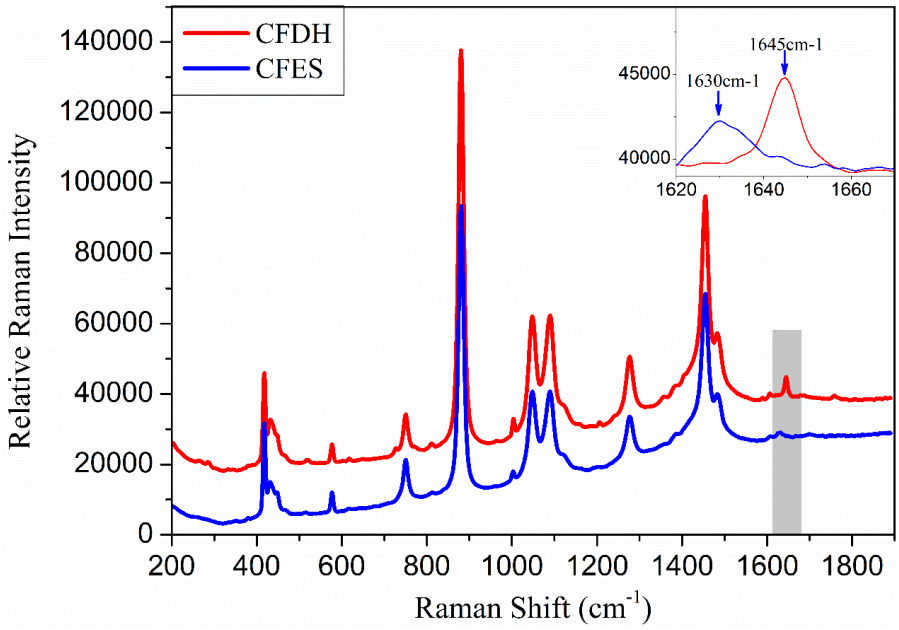

Figure 4. Raman spectra of CFDH and CFES in ethanol-water mixed mixtures showing "finger printing" region (see inset) at 1630 cm-1 and 1645 cm-1 for CFES and CFDH, respectively.

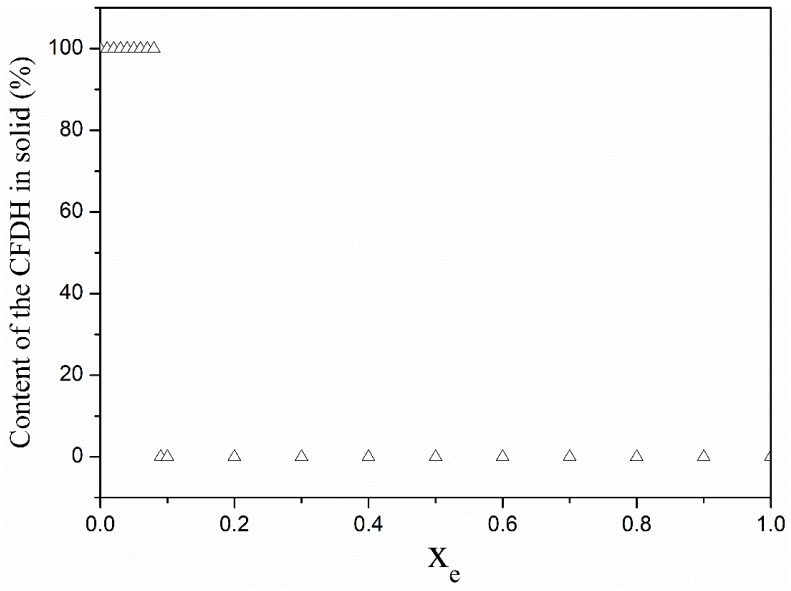

Figure 5. The phase transformation profile identified by PXRD after 24 h for CFDH and CFES in ethanol-water mixtures at 298.15 K.

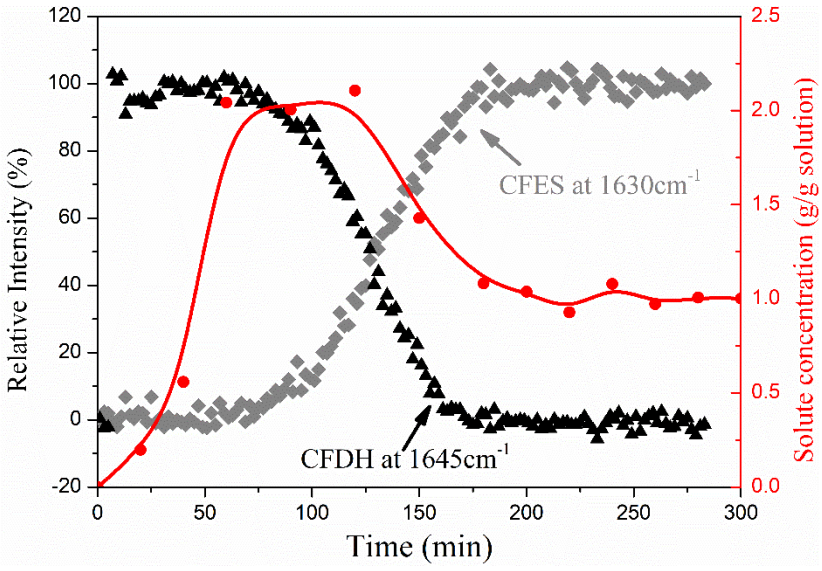

Figure 6. Relative intensities of Raman peaks at 1630 cm^{-1} for CFES (grey line) and Raman peak at 1645 cm^{-1} for CFDH (black line) and the solution concentration (red line) measured by UV spectroscopy.

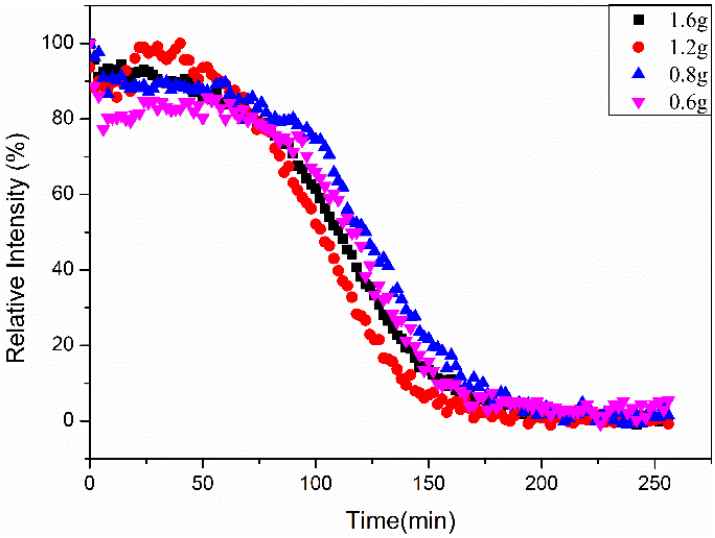

Figure 7. Time-dependent Raman intensity data showing the influence of solid loading on transformation time from CFDH to CFES in ethanol-water mixed at 298.15 K.

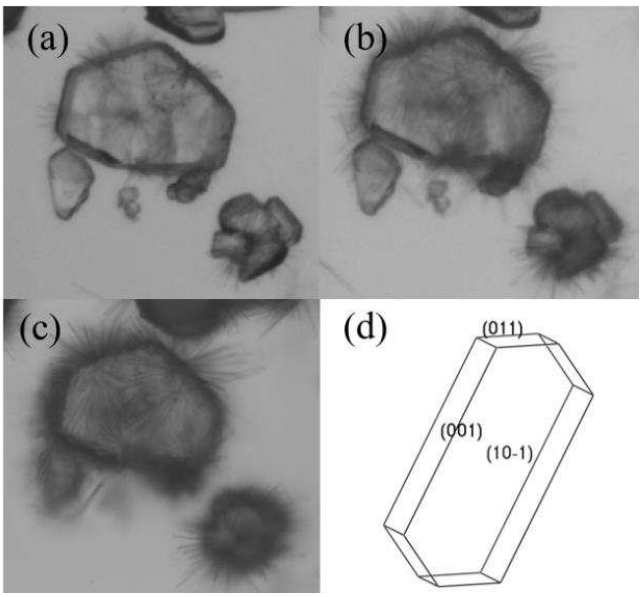

Figure 8. Time-dependent epitaxial nucleation and growth of CFES on the surfaces of a single crystal of CFDH optical micrographs: (a) 0.5 min; (b) 1.0 min; (c) 2 min; (d) schematic showing the crystal morphology of CFDH.

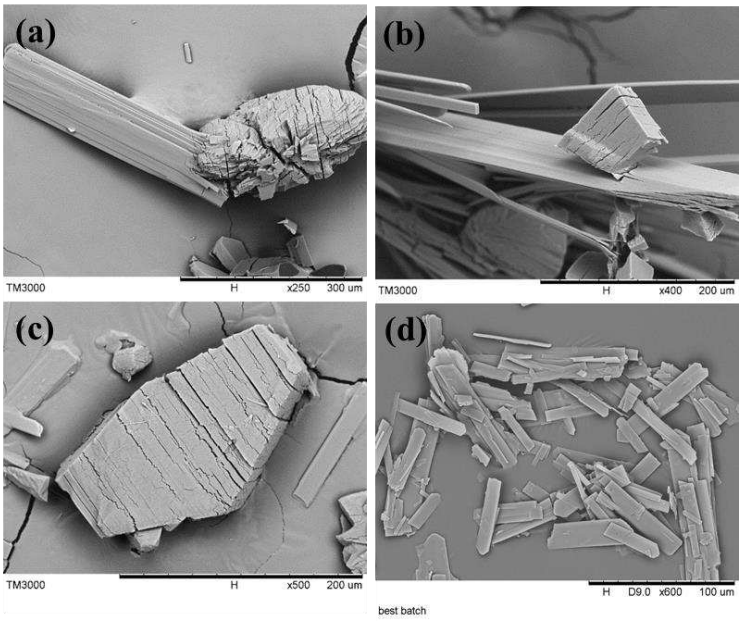

Figure 9. SEM micrographs of (a) CFES epitaxial growth on the surface of CFDH, (b) CFDH epitaxial on the surface of CFES, (c) CFDH and (d) CFES.

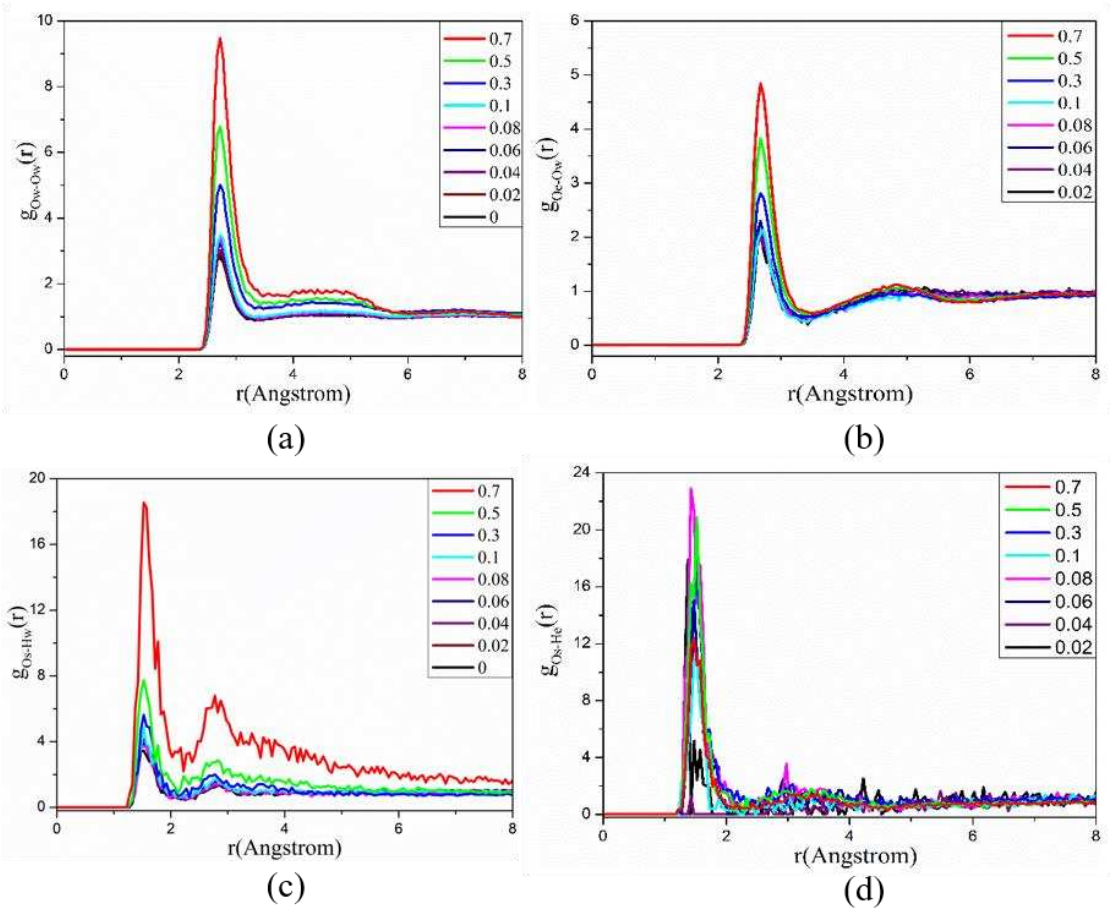

Figure 10. The *g(r)* radial distribution function plots for MD simulations highlighting intermolecular interactions: (a) O_w-O_w; (b) O_e-O_w; (c) O_s-H_w; (d) O_s-H_e where O is for oxygen and the sub-script refer to water (w), ethanol (e) and the solute molecule (s). The mole fraction of ethanol is from 0 to 0.7 in ethanol-water mixtures.

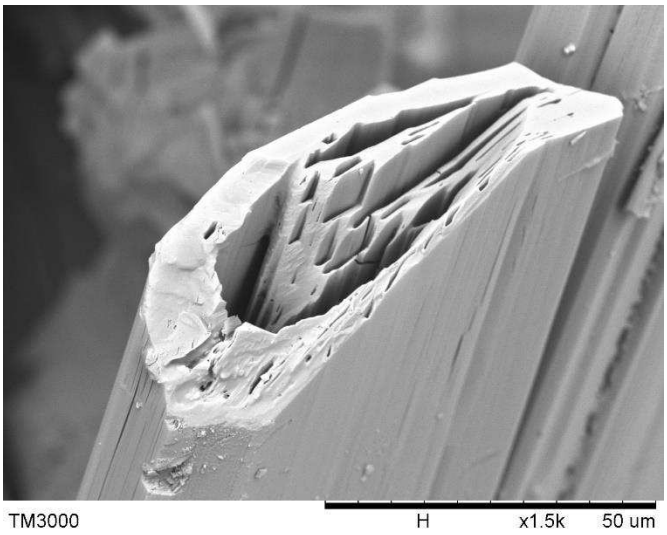

Figure 11. SEM micrograph of the crystal of CFES showing a hollow channel existed in the structure consistent with the MD simulation results that a water cluster formed in ethanol-water mixture.

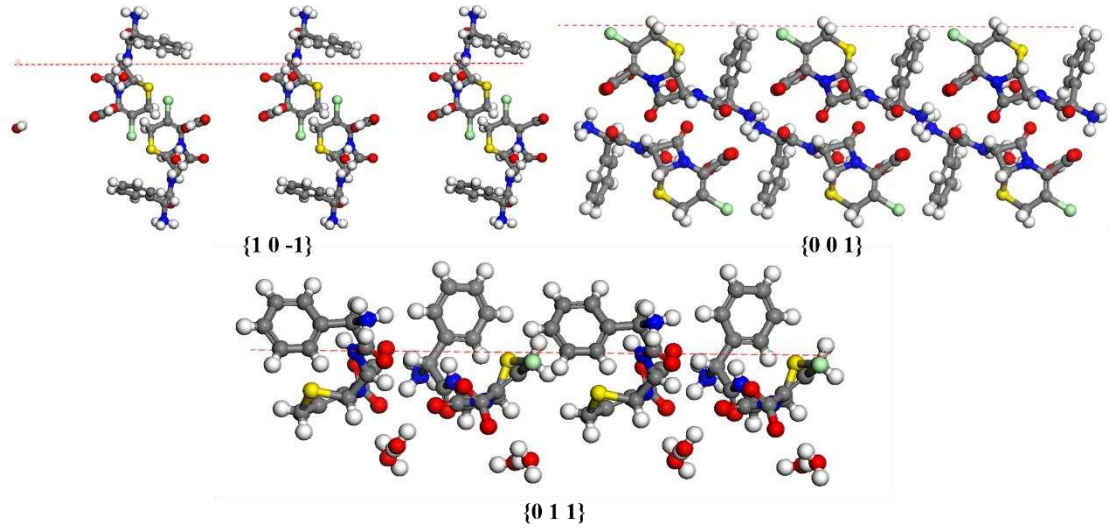

Figure 12. Intermolecular packing diagrams showing the surface termination chemistry of the {10-1}, {001} and {011} planes.

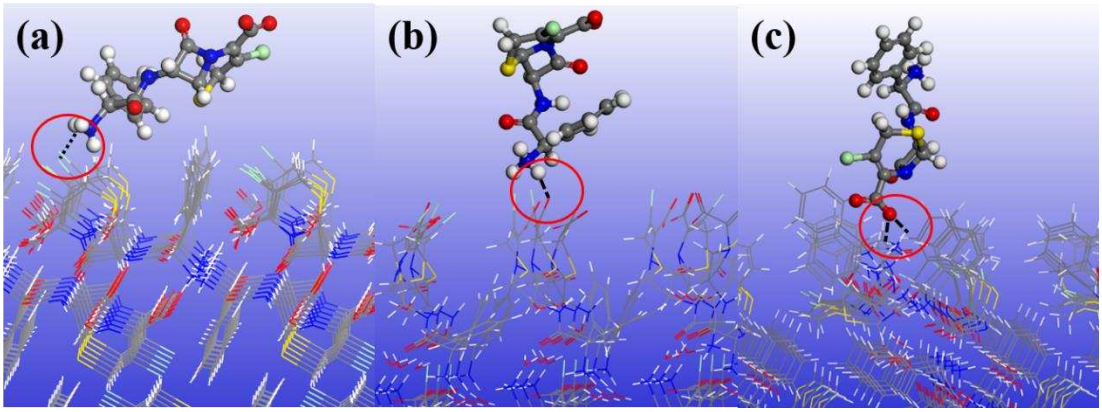

Figure 13. Surface chemistry for the dominant crystal habit planes for CFDH showing the optimal adsorption binding site for single molecules of cefaclor: (a) face {001}, (b) face {10-1}, and face {011}.

Table 1. The coordination number of $g_{Os\text{-}Hw}(r)$ and $g_{Os\text{-}He}(r)$ plots showing the abrupt increases of ethanol molecules while a rapidly decreased of water molecules surround solute molecule when the ethanol content change from x_e=0.1 to x_e=0.3.

Interaction	Coordination number								
Types	0	0.02	0.04	0.06	0.08	0.1	0.3	0.5	0.7
$g_{Os\text{-}Hw}(r)$	1.64	1.48	1.63	1.41	1.43	1.51	1.09	0.89	1.00
$g_{Os\text{-}He}(r)$	0	0.03	0.07	0.22	0.45	0.23	1.03	1.32	1.10

Table 2. Mean adsorption energy ($kcal \cdot mol^{-1} \cdot nm^{-2}$) of the molecules on the surfaces of CFDH.

Surfaces of CFDH	{0 1 1}	{0 0 1}	{1 0 -1}
Mean Adsorption Energy ($kcal \cdot mol^{-1} \cdot nm^{-2}$)	-18.41	-17.94	-16.69

For Table of Contents Use Only

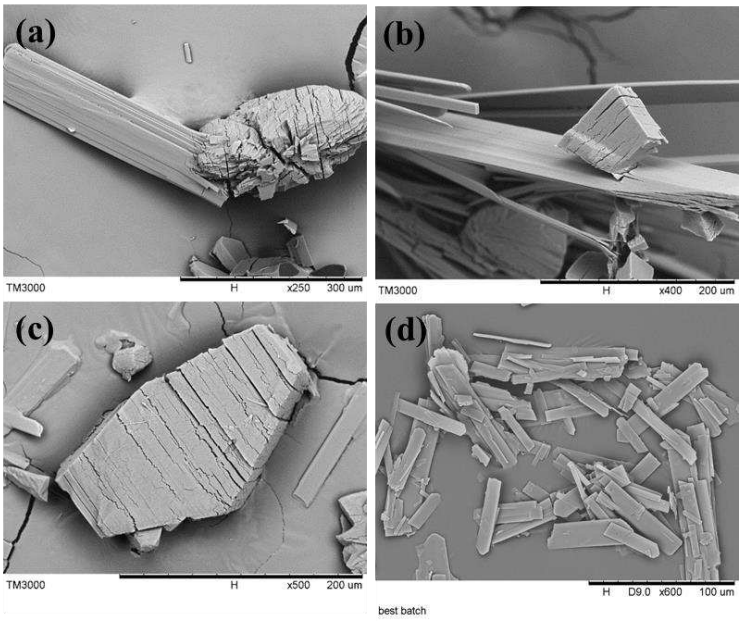

Synopsis: The needle-like crystal of cefaclor ethanol-water solvate consistently nucleation on the surface of cefaclor dihydrate during the solution-mediated phase transformation process, and vice versa.